Electronic Supplementary Information (ESI) for: Simultaneous Enhancement of Electrical Conductivity and Thermopower in Bi_2S_3 Under Hydrostatic Pressure

Tribhuwan Pandey and Abhishek K. Singh*

Materials Research Centre, Indian Institute of Science, Bangalore - 560012, India

I. PBE BAND STRUCTURES WITHOUT SPIN ORBIT COUPLING:

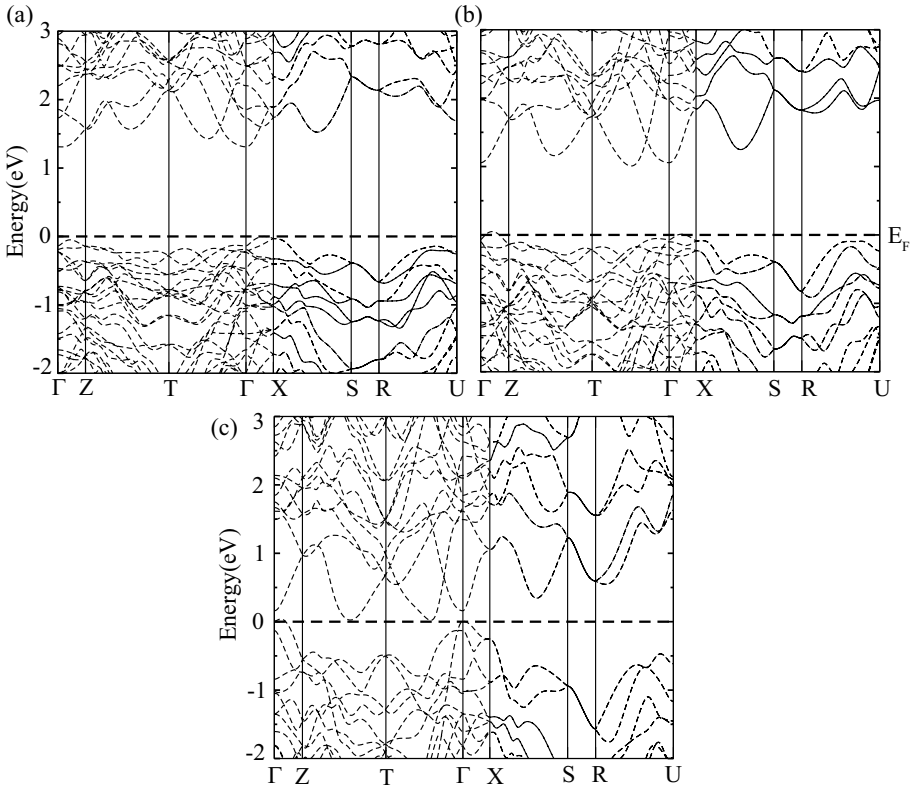

Figure S1: PBE band structure without spin orbit coupling at (a) 0, (b) 10, and (c) 17 GPa pressure.

II. BADER CHARGE ANALYSIS AND CHARGE TRANSFER

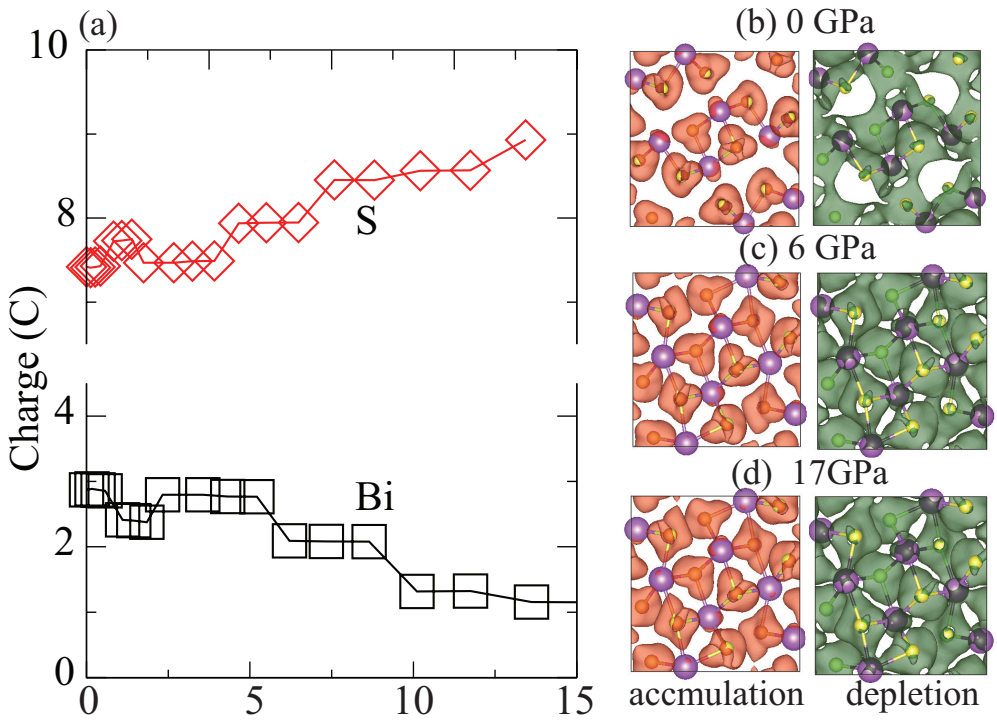

Figure S2: (a) Average Bader charge of Bi and S as a function of hydrostatic pressure. Isosurfaces of charge accumulation (red) and depletion (green) of Bi_2S_3 at hydrostatic pressure of (b) 0, (c) 7, and (d) 17 GPa.

III. DENSITY OF STATES AND CONDUCTIVITY EFFECTIVE MASS:

For non parabolic bands, the effective mass becomes energy dependent $m_{dos} = m(E)$ and can be calculated by density of states and its energy derivative as [1, 2]

$$m_{dos}(E) = m_e m^*_{dos}(E) = \hbar^2 \sqrt[3]{\pi^4 g(E) g\prime(E)} \tag{1}$$

where $g(E)$ and $g\prime(E)$ are density of states and its energy derivative.

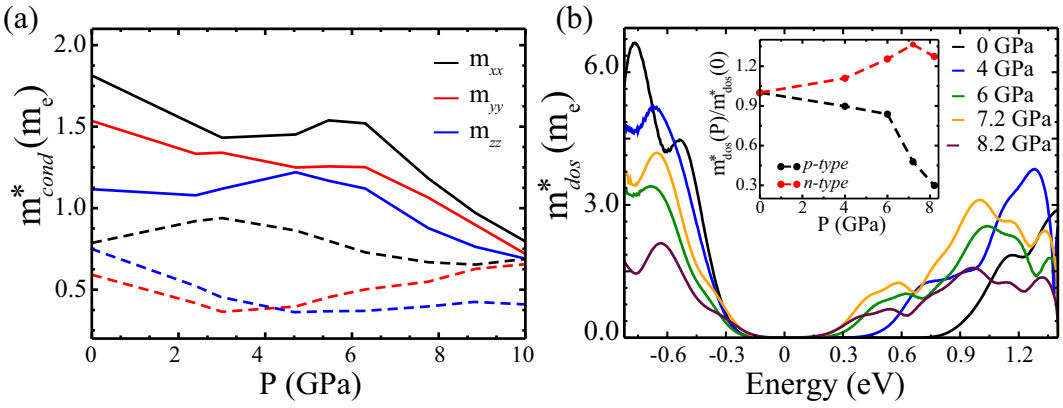

Figure S3: (a) Conductivity effective mass as a function of hydrostatic pressure at carrier concentration 10^{20} cm^{-3} at T=800 K. (b) DOS effective mass of carriers near the band edges in Bi_2S_3 at different pressures. Inset shows variation in effective mass as a function of pressure at carrier concentration of 10^{20} cm^{-3} and T=800 K. These values are scaled with respect to 0 GPa pressure.

IV. DIRECTIONAL DEPENDENT THERMOPOWER

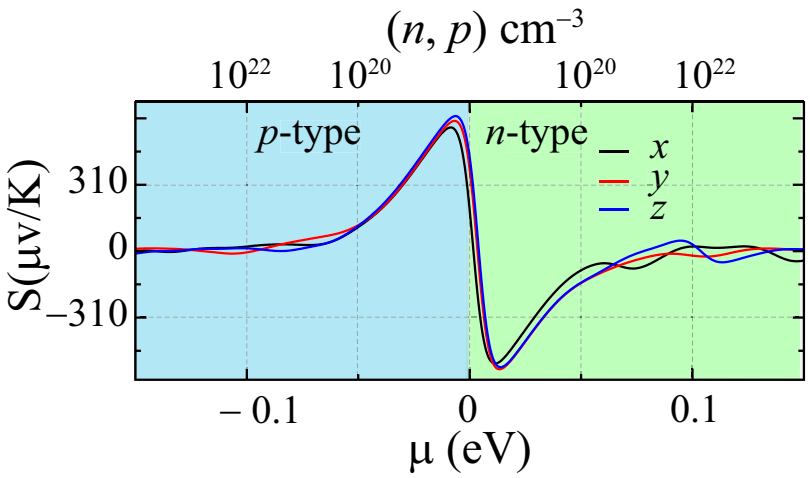

Figure S4: The thermopower for unstrained Bi_2S_3 as a function of chemical potential at 300 K (positive and negative values correspond to electrons and holes). Top X-axis is marked with the corresponding equivalent carrier concentration.

V. PRESSURE DEPENDENT TRANSPORT PROPERTIES AT 300 AND 600 K

To confirm the observed enhancement in power factor under pressure, we performed transport calculation at 300 and 600 K. Irrespective of the temperature, we observe enhancement in thermopower at low pressures under n-type doping. A very week dependence of thermopower on pressure for p-type doping was observed. Combining this with the trend in conductivity leads to the enhancement in power factor, which is independent of temperature.

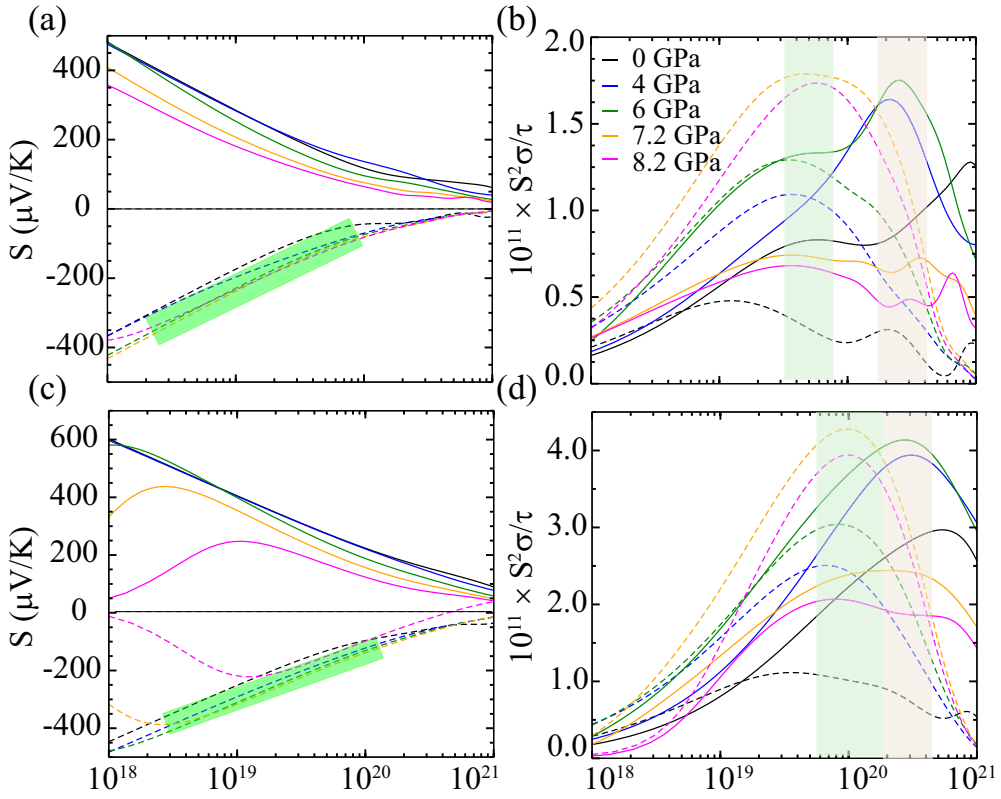

Figure S5: Transport coefficients of Bi_2S_3 under different pressure as a function of carrier concentration. (a) Thermopower, (b) power factor with respect to relaxation time at 300 K, (c) thermopower, and (d) power factor with respect to relaxation time at 600 K. The shaded region in the figure (b) and (d) denotes the range of optimal carrier concentration. Solid and dotted lines show p- and n-type of carriers, respectively.

VI. PHONON DISPERSION AT HIGH PRESSURE

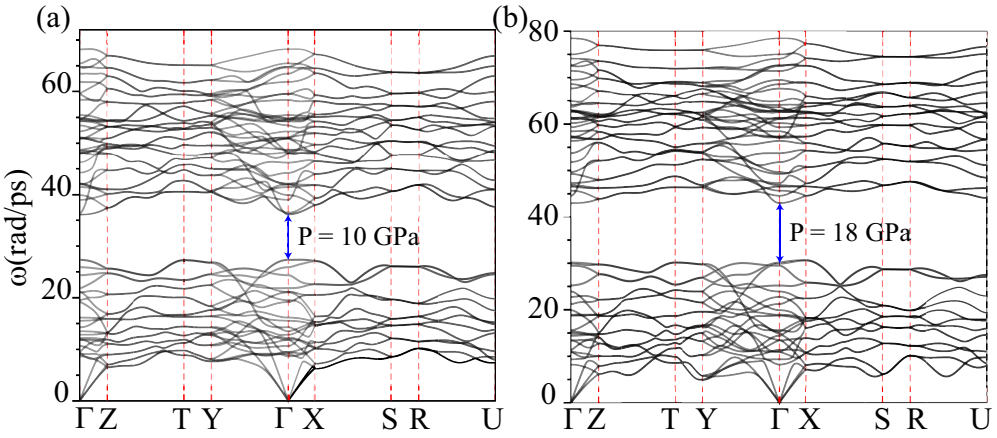

Figure S6: Phonon dispersions for Bi_2S_3 at (a) P = 10 and (b) P = 18 GPa. Note that the phononic gap in the optical branch increases with increasing pressure. The absence of negative frequency in the phonon dispersion indicates dynamical stability of the structure.

VII. RELAXATION TIME AND FIGURE OF MERIT UNDER PRESSURE

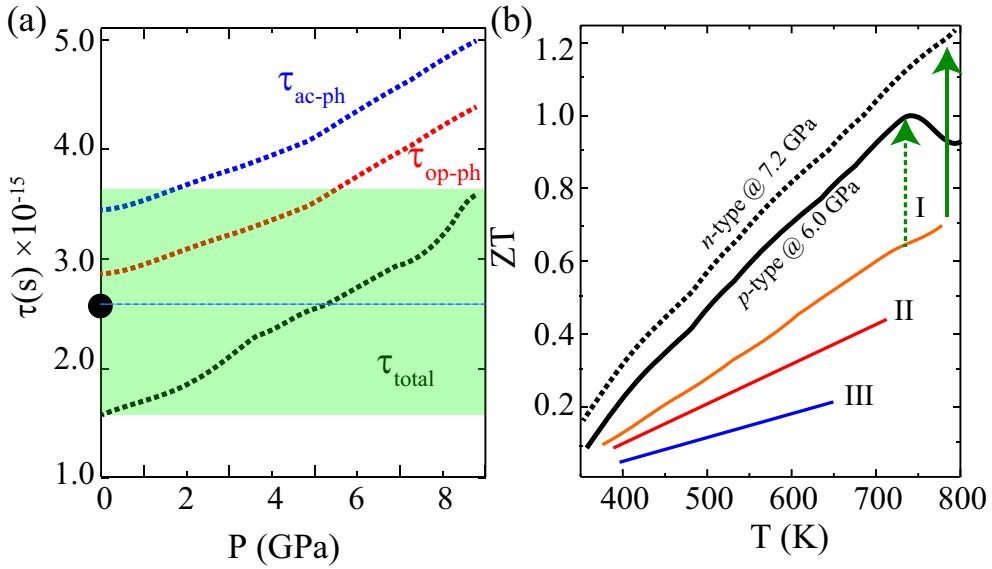

Figure S7: Pressure dependent relaxation time calculated by considering contribution form acoustical and polar optical phonon scattering [3–5]. The circle denotes the relaxation time obtained by comparing σ/τ with experimental σ of Mizoguchi *et.al* [6]. τ does not vary significantly as a function of pressure as shown by shaded area. (b) Figure of merit of Bi_2S_3 under pressure as a function of temperature for p- and n-type carriers at 6 and 7.2 GPa

pressure. The previously reported values are also shown for better comparison. Application of pressure leads to two time enhancement in ZT. The line denoted by I, II, III is the experimental data from references [7–9], respectively.

VIII. EFFECT OF DOPING ON ELECTRONIC STRUCTURE AND PHONON DISPERSIONS

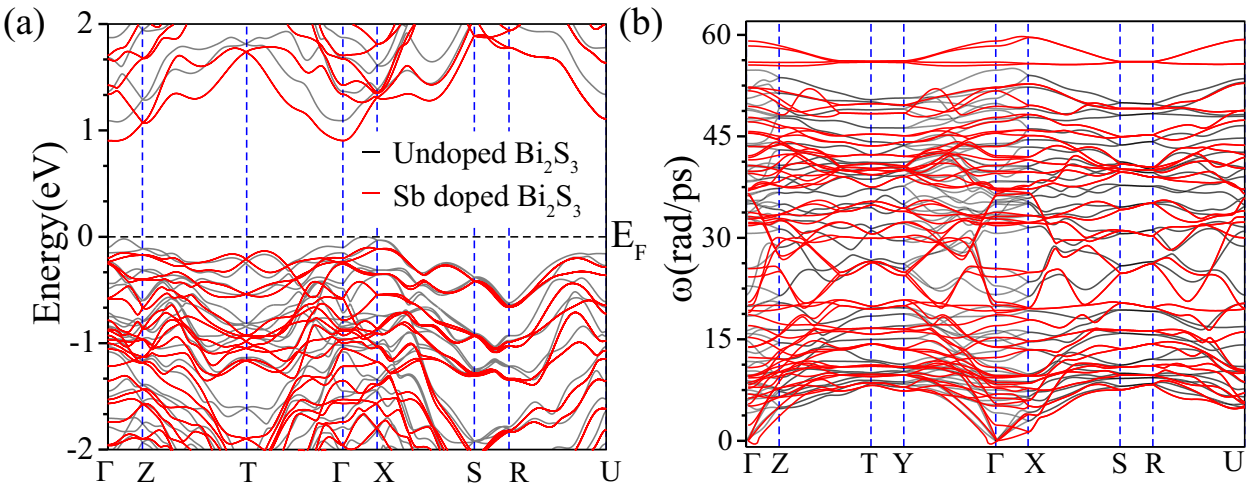

Figure S8: (a) Band structure and (b) phonon dispersion for Sb doped Bi_2S_3. For comparison the results for undoped Bi_2S_3 is also shown. Similar to application of hydrostatic pressure doping results in a decrease in the band gap. Also under doping there is significant softening of acoustical phonons near the zone center (Γ).

[1] K Kutorasinski, B Wiendlocha, J Tobola, and S Kaprzyk, "Importance of relativistic effects in electronic structure and thermopower calculations for Mg_2Si, Mg_2Ge, and Mg_2Sn," Phys. Rev. B **89**, 115205 (2014).

[2] K Kutorasinski, B Wiendlocha, S Kaprzyk, and J Tobola, "Electronic structure and thermoelectric properties of n-and p-type SnSe from first-principles calculations," Phys. Rev. B **91**, 205201 (2015).

[3] DI Bilc, SD Mahanti, and MG Kanatzidis, "Electronic transport properties of PbTe and $AgPb_mSbTe_{2+m}$ systems," Phys. Rev. B **74**, 125202 (2006).

[4] A Popescu, LM Woods, J Martin, and GS Nolas, "Model of transport properties of thermoelectric nanocomposite materials," Phys. Rev. B **79**, 205302 (2009).

[5] Daniel I Bilc, Geoffroy Hautier, David Waroquiers, Gian-Marco Rignanese, and Philippe Ghosez, "Low-dimensional transport and large thermoelectric power factors in bulk semiconductors by band engineering of highly directional electronic states," Phys. Rev. Lett. **114**, 136601 (2015).

[6] H Mizoguchi, H Hosono, N Ueda, and H Kawazoe, "Preparation and electrical properties of Bi_2S_3 whiskers," J. Appl. Phys. **78**, 1376–1378 (1995).

[7] Kanishka Biswas, Li-Dong Zhao, and Mercouri G Kanatzidis, "Tellurium-free thermoelectric: The anisotropic n-type semiconductor Bi_2S_3," Adv. Energy Mater. **2**, 634–638 (2012).

[8] Li-Juan Zhang, Bo-Ping Zhang, Zhen-Hua Ge, and Cheng-Gong Han, "Fabrication and properties of $Bi_2S_{3-x}Se_x$ thermoelectric polycrystals," Solid State Commun. **162**, 48–52 (2013).

[9] Zhen-Hua Ge, Bo-Ping Zhang, Yi-Qiang Yu, and Peng-Peng Shang, "Fabrication and properties of $Bi_{2-x}Ag_{3x}S_3$ thermoelectric polycrystals," J. Alloys Compd. **514**, 205–209 (2012).